



**HAL**  
open science

## Domain structure and energy losses up to 10 kHz in grain-oriented Fe-Si sheets

A. Magni, A. Sola, Olivier de La Barriere, Enzo Ferrara, Luca Martino, C. Ragusa, C. Appino, F. Fiorillo

► **To cite this version:**

A. Magni, A. Sola, Olivier de La Barriere, Enzo Ferrara, Luca Martino, et al.. Domain structure and energy losses up to 10 kHz in grain-oriented Fe-Si sheets. *AIP Advances*, 2021, 11 (1), pp.015220. 10.1063/9.0000184 . hal-03316102

**HAL Id: hal-03316102**

**<https://hal.science/hal-03316102>**

Submitted on 6 Aug 2021

**HAL** is a multi-disciplinary open access archive for the deposit and dissemination of scientific research documents, whether they are published or not. The documents may come from teaching and research institutions in France or abroad, or from public or private research centers.

L'archive ouverte pluridisciplinaire **HAL**, est destinée au dépôt et à la diffusion de documents scientifiques de niveau recherche, publiés ou non, émanant des établissements d'enseignement et de recherche français ou étrangers, des laboratoires publics ou privés.

# Domain structure and energy losses up to 10 kHz in grain-oriented Fe-Si sheets

A. Magni<sup>1</sup>, A. Sola<sup>1</sup>, O. de la Barrière<sup>2</sup>, E. Ferrara<sup>1</sup>, L. Martino<sup>1</sup>, C. Ragusa<sup>3</sup>, C. Appino<sup>1</sup>, F. Fiorillo<sup>1</sup>

<sup>1</sup>*Advanced Materials Metrology and Life Science Division, INRIM, Torino, Italy*

<sup>2</sup>*Lab. SATIE, CNRS-ENS, Saclay, France*

<sup>3</sup>*Energy Department, Politecnico di Torino, Torino, Italy.*

## Abstract

We investigate in theory and experiment the frequency dependence of magnetic losses in Grain-Oriented 0.29 mm thick high-permeability steel sheets up to 10 kHz. Such unusually broad frequency range, while responding to increasing trends towards high-frequency regimes in applications, is conducive to a complex evolution of the magnetization process, as imposed by increasing frequencies to a non-linear high-permeability saturable material. We show that the concept of loss decomposition, supported by observations of the domain wall dynamics through Kerr experiments, is effective in the assessment of the broadband frequency dependence of the energy loss. By calculating, in particular, the instantaneous and time averaged macroscopic induction profiles across the sheet thickness through the Maxwell's diffusion equation, the classical loss component  $W_{\text{class}}$ , versus frequency  $f$  and peak polarization  $J_p$  is obtained. Instrumental to a simplified theoretical approach is the assumption of the normal magnetization curve as the magnetic constitutive equation of the material. While the hysteresis loss  $W_{\text{hyst}}$  invariably increases with frequency, the excess loss  $W_{\text{exc}}$ , the quantity directly associated with the eddy currents circulating around the moving domain walls, tends to vanish upon increasing both frequency and induction values. The Kerr experiments actually show that, while the oscillating  $180^\circ$  domain walls can adjust to the depth of the induction profile by bowing at low  $J_p$  values, the magnetization reversal at high inductions and frequencies occurs by inwardly motion of symmetric fronts originating at the sheet surface, according to a classical framework.

1

## 2 **I. Introduction**

3       Recent trends in electrical energy generation and transmission are guided by the growing role of  
4 heterogeneous and distributed renewable sources. New technologies, associated with the concept of  
5 “smart grids”, are therefore developed, in order to flexibly accommodate the supply and conversion of  
6 energy.<sup>1,2</sup> Under these circumstances, the traditional applications of the 50 – 60 Hz power transformers  
7 combine with the operation of newly introduced devices, like the solid state transformers, where high  
8 frequencies and electronic controls, introducing high harmonic contents, provide a novel operating  
9 landscape. Consequently, the conventional paradigms underlying the investigation and development  
10 of the grain-oriented (GO) Fe-Si alloys need to evolve and widen their range.<sup>3</sup> Transformers employed  
11 in power electronics operate, for example, at kHz frequencies, with high order harmonics generated by  
12 Pulse Width Modulation (PWM).<sup>4</sup> In rotating electrical machines, GO sheets can provide an interesting  
13 alternative to the conventional non-oriented (NO) Fe-Si alloys.<sup>5</sup> It is thus shown that very high speed  
14 motors display better efficiency and higher working inductions when the stator core is built by suitable  
15 combination of GO and NO sheets.<sup>6</sup> However, the whole matter of high-frequency response of GO  
16 alloys and its quantitative interpretation have not been assessed so far. The prevalent attitude to this  
17 problem is one of resorting to empirical models and formulations, like the Steinmetz’s equation.<sup>7-9</sup> The  
18 phenomenology of energy losses at high frequencies has actually been brought to physical treatment  
19 in NO sheets, taking advantage of the fine scale of the domain structure. Here, the Maxwell’s diffusion  
20 equation was solved by a Finite Element Method (FEM), with the magnetic constitutive law derived  
21 from a dynamic hysteresis model.<sup>10-12</sup> It is a relatively complex approach, where one assumes that the  
22 statistics of the moving domain walls (dw) applies at the scale of the single finite element, which is  
23 small compared to the sheet thickness. This procedure is difficult to justify in the case of GO sheets  
24 and their broad domain structure.<sup>13</sup> It was suggested that, where high peak polarization values are  
25 involved in GO Fe-Si (near rectangular loop), a step-like (saturating) magnetic constitutive law coupled  
26 to the Maxwell’s diffusion equation, to be solved numerically<sup>14</sup> or analytically<sup>15</sup>, applies at all  
27 frequencies. The envisaged magnetization process consists, in this case, of symmetric reversal fronts,  
28 propagating inwards from the sheet opposite surfaces to the midplane.<sup>16</sup> The Kerr observations show,  
29 however, that this does not happen at power frequencies, where the longitudinal bar-like domain  
30 structure always survives, whatever the peak polarization.

31       In this paper, we discuss the broadband ( $DC \leq f \leq 10$  kHz) frequency dependence of the energy  
32 losses measured in 0.29 mm thick high-permeability GO sheets subjected to sinusoidal polarization of  
33 peak values  $J_p$  ranging between 100 mT and 1.70 T. We first calculate the macroscopic response of the  
34 material in terms of induction profiles across the sheet thickness and classical loss  $W_{\text{class}}(f)$ , using the

35 electromagnetic diffusion equation and its solution. The calculation is performed by means of a simple  
 36 numerical model, lumping in the normal magnetization curve the constitutive equation of the material.  
 37 This permits us to separately determine the frequency dependent hysteresis  $W_{\text{hyst}}(f)$  and excess  $W_{\text{exc}}(f)$   
 38 loss components and their evolution under increasing skin effect. Such evolution is measured against  
 39 the direct findings on the dw dynamics provided by stroboscopic Kerr observations. These consistently  
 40 show how the dw bowing, accommodating for deepening induction profile with frequency at low  
 41 inductions, makes way for symmetrical reversal fronts, propagating from the sheet surface towards  
 42 mid-plane, at high inductions.

## 43 **II. A classical model for the skin effect and losses**

### 44 *A. The induction profile*

45 The eddy currents circulating in a lamination under steady dynamic excitation are assumed to  
 46 form a macroscopic pattern, investing the whole cross-sectional area, and localized patterns,  
 47 surrounding the moving dws. The macroscopic currents are the result of the diffusion and superposition  
 48 of the localized eddies and concentrate towards the sheet surface. The ensuing counterfield, combining  
 49 with the uniform applied field, does impose, at any instant of time, a definite macroscopic profile  $J(x)$   
 50 to the magnetization across the sheet thickness, with obvious fluctuations at the scale of the domains.  
 51 These will rearrange and adjust by the motion of the dws to such a profile. While the evolution of  $J(x)$   
 52 versus time, responsible for the homogeneous response of the material, is associated with  $W_{\text{class}}(f)$ , the  
 53 superimposed fluctuations, with their localized currents, give rise to the extra dynamic contribution  
 54  $W_{\text{exc}}(f)$ . Let us then express the relationship between macroscopic magnetic induction  $b(x,t)$  and  
 55 magnetic field  $h(x,t)$  at any frequency and peak induction value as a function of the spatial coordinate  
 56  $x$  across the sheet thickness  $d$  ( $-d/2 \leq x \leq d/2$ ) according to the classical treatment by the Maxwell's  
 57 diffusion equation

$$58 \quad \frac{\partial^2 h}{\partial x^2} - \sigma \frac{\partial b}{\partial t} = 0 \quad , \quad (1)$$

59 with the boundary conditions at mid-plane and surface

$$60 \quad \frac{\partial h}{\partial x} \Big|_{x=0} = 0 \quad , \quad \frac{\partial h}{\partial x} \Big|_{x=\pm d/2} = \sigma \frac{d}{2} \frac{dB}{dt} \quad (2)$$

61 where  $\sigma$  is the conductivity and  $B(t)$  is the instantaneous induction of peak value  $B_p$  averaged over the  
 62 sheet thickness.

63 To actual constitutive relation  $b(h)$  is hysteretic in nature and its use in (1) would require a  
 64 cumbersome numerical procedure.<sup>10, 11</sup> To simplify the matter, we identify here the magnetic  
 65 constitutive law with the normal magnetization curve. Equation **Erreur ! Source du renvoi**  
 66 **introuvable.** is then solved by standard finite elements calculations, using the fixed point method.<sup>10, 11</sup>  
 67 The sheet thickness is subdivided in 100 layers and the macroscopic profile  $J(x, t)$  of the polarization  
 68 is calculated at any instant of time, for any measured  $J_p$  value, at the measuring frequencies. Fig. 1  
 69 provides an example of the classically predicted behavior of the local peak polarization  $J_p(x)$  across  
 70 the sheet thickness at low inductions (average  $J_p = 0.25$  T). Lack of flux penetration can be appreciated

71 in this case on increasing the frequency beyond about 200 Hz. The sheet interior soon attains a state of  
 72 near-zero magnetization upon further frequency increase and at 10 kHz the magnetization change is  
 73 predicted to occur within a  $\sim 50 \mu\text{m}$  thick surface layer. With higher (thickness averaged)  $J_p$  values,  
 74 however, the magnetization tends to approach the saturated state at the surface and the predicted  $J_p(x)$   
 75 profile takes a sharper shape (see inset in Fig. 1). At  $f = 10 \text{ kHz}$  and  $J_p = 1.0 \text{ T}$ , a neat separation is, for  
 76 example, seen to occur across the sheet thickness between an outer active region and an inner dead  
 77 core. At very high inductions we eventually fall in the classical problem of magnetization reversal in a  
 78 highly nonlinear material.<sup>14-17</sup> Fig. 2, concerning the classical eddy current calculation at  $f = 10 \text{ kHz}$   
 79 and  $J_p = 1.7 \text{ T}$ , shows how reversal fronts are created and predicted to symmetrically proceed from the  
 80 opposite sheet surfaces towards the sheet mid-plane along any semi-cycle. It is also shown how the  
 81 local  $J_p(x)$  eventually suffers only a slight depression at  $x = 0$ , as imposed by the need to reach high  $J_p$   
 82 . The front wave phenomenon actually appears, in this case, to be a specifically high-frequency effect,  
 83 at odds with the similar effect postulated to occur in highly homogeneous materials (e.g. fine-grained  
 84 non-oriented alloys) also at low frequencies. Kerr observations at power frequencies show that, even  
 85 when it is cycled between  $\pm J_p$  values not far from saturation (e.g.  $J_p/J_s = 0.91$ ), a GO sheet exhibits the  
 86 typical mechanisms of nucleation and growth of longitudinal domains by  $180^\circ$  dw motion.<sup>18</sup> The  
 87 question appears then one of understanding the role of the dw's across a broad range of frequencies and  
 88 the way the magnetization process can eventually end into a near-classical behavior. The question then  
 89 arises of the phenomenology of magnetic losses and the way it can be assessed. It is in any case  
 90 immediate to obtain in all cases, via the solutions of (1) and use of the Poynting theorem, or,  
 91 equivalently, the integration of the square of the current density on the sheet thickness, the classical  
 92 loss component  $W_{\text{class}}(J_p, f)$ .

### 94 III. Experimental method

95 A 0.29 mm thick high-permeability Fe-Si GO alloy (M2H type) was subjected to static and dynamic  
 96 characterization up to 10 kHz. The measurements were performed on 300 mm long Epstein strips under  
 97 controlled sinusoidal induction waveform, making use of a calibrated hysteresisgraph-wattmeter.<sup>19</sup>  
 98 Two different magnetizer configurations were adopted. First, an appropriate number of strips was  
 99 tested by the conventional Epstein frames, according to the standards IEC 60404-2 and IEC 60404-10.  
 100 By this method, the lowest  $J_p$  values (100 mT and 250 mT) could be covered till 10 kHz. In order to  
 101 deal with manageable signals, the upper  $J_p$ - $f$  right corner was investigated by a single-strip tester, where  
 102 the longitudinal GO strip, surrounded by a single layer magnetizing solenoid, is inserted between the  
 103 pole faces of a laminated double-C yoke. A few-turn secondary coil is tightly wound at the strip centre  
 104 and an  $H$ -coil is placed on top of it. The turns of the windings are all properly spaced, in order to avoid  
 105 capacitive effects in the kilohertz range and single shot measurements guarantee negligible sample  
 106 heating. A detailed description of this setup is provided in Ref..<sup>20</sup> A sufficiently wide overlapping  $J_p -$   
 107  $f$  region could be covered with both Epstein frame and single-strip  $H$ -coil method, within  $\pm 2 \%$

108 agreement between the respective loss figures. The full DC normal magnetization curve was obtained  
109 by a point-by-point method.

110 Dynamic Kerr observations were carried out by means of stroboscopic imaging. The  
111 magneto-optical setup employs an X-Cite series 120 lamp whose light is filtered, polarized and detected  
112 by a gated intensified charge-coupled device (CCD) camera (Picostar LaVision). This permits one to  
113 acquire equally time-spaced images at given frequency along the magnetization loop. The acquisition  
114 is triggered by a signal with an adjustable phase with respect to the signal that drives the magnetization  
115 of the sample. The signals are controlled by an Agilent 33522A function generator and visualized by  
116 means of a LeCroy 816Zi oscilloscope. The magnetization of the sample, which is subjected to a tensile  
117 stress of 9 MPa, is guaranteed by a split solenoid powered by a NF HSA4052 DC to 500kHz bipolar  
118 amplifier. The sample induction is detected by means of a 3-turn pickup coil, wound close to the  
119 investigated specularly polished area. Each magneto-optical image (resolution 0.5  $\mu\text{m}/\text{pix}$ ), detected  
120 on a 5 mm diameter spot, is the average of 9000 frames, from which the usual background subtraction  
121 subtraction is made. The sample temperature, monitored by a Pt100 resistance thermometer, was  
122 allowed to rise during acquisition by a maximum of 15  $^{\circ}\text{C}$ .

123

### 124 **III. Magnetic losses, domains wall dynamics, and their frequency evolution**

125

126 Whatever the frequency range, the domain structure, and the skin depth, the energy loss  
127 decomposition method invariably applies to the analysis of the magnetic losses. It requires, as a first  
128 step, the calculation of the classical loss component. As the  $J_p(x)$  profiles in Fig. 1 suggest, the standard  
129 analytical formula  $W_{\text{class}} = \left(\frac{\pi^2}{6}\right)\sigma d^2 J_p^2 f$ , requiring uniform induction, does not apply in these GO  
130 sheets above a few hundred Hz. We are therefore obliged to resort to more complex approaches, like  
131 the one discussed in the previous section. Relying then on the abovementioned calculations, we can  
132 proceed to the broadband loss decomposition, examples of which are shown in Fig. 3a and 3b. These  
133 refer to low ( $J_p = 0.25$  T) and high ( $J_p = 1.70$  T) induction values, respectively. It is apparent in these  
134 figures that, with the emergence of the skin effect, the paths followed by  $W_{\text{hyst}}$ ,  $W_{\text{class}}$ , and  $W_{\text{exc}}$  at high  
135 frequencies are quite different at low and high inductions. In particular,  $W_{\text{exc}}$  and  $W_{\text{class}}$  dominate for  $J_p$   
136  $= 0.25$  T and  $J_p = 1.70$  T, respectively, while the increase of  $W_{\text{hyst}}$ , while relevant at the lowest  
137 inductions, always plays a minor role.

138 The starting point for the loss analysis is the previously discussed calculation of  $W_{\text{class}}$ , as  
139 derived, together with the  $J_p(x)$  profile, from the diffusion equation (1). It is apparent, looking at the  
140 profiles, that  $W_{\text{hyst}}$  will increase together with  $J_p(x)$  on going from the sheet core to the surface. At low  
141 frequencies, where the skin effect is not an issue, the hysteresis loss  $W_h(J_p)$  is frequency independent,  
142 and can be obtained according to a straightforward extrapolation of the measured loss to zero  
143 frequency.<sup>21</sup> On the other hand, the present experiments show that a power law  $W_{\text{hyst}} = kJ_p^\alpha$  for the  
144 dependence of  $W_{\text{hyst}}$  on  $J_p$  applies, with  $k = 14.15$  and  $\alpha = 1.85$  up to  $J_p = 1.5$  T and  $k = 15.6$  and  $\alpha =$

145 2.95 at higher  $J_p$  values (loss units in  $J/m^3$ ). By taking into account that the quasi-static loss  $W_{\text{hyst}}$  is  
 146 generated by very localized dissipative dw processes (Barkhausen jumps), we can easily retrieve its  
 147 contribution at any frequency and average  $J_p$  value by integrating the local  $W_{\text{hyst}}$  along the  $J_p(x)$  profile  
 148

$$149 \quad W_{\text{hyst}}(J_p, f) = \frac{1}{d} \int_{-d/2}^{d/2} k J_p^\alpha(x) dx. \quad (2)$$

150

151 Once  $W_{\text{class}}(f)$  and  $W_{\text{hyst}}(f)$  are calculated, the excess loss component  $W_{\text{exc}}(f) = W(f) - W_{\text{hyst}}(f) - W_{\text{class}}(f)$ ,  
 152 where  $W(f)$  is the measured energy loss, is obtained at all  $J_p$  values.

153 Looking at the examples shown in Fig. 3, one can see how the prediction of the statistical  
 154 theory of losses, where, for given  $J_p$ ,  $W_{\text{hyst}}$  is constant,  $W_{\text{class}}(f)$  is, as previously recalled, a linear  
 155 function of  $f$ , and  $W_{\text{exc}}(f)$  is analytically formulated via defined statistical parameters,<sup>22</sup> does not fully  
 156 apply beyond about 200 Hz. It is observed, in particular, how the theoretical  $W_{\text{exc}}(f)$  (STL line), deviates  
 157 from the obtained  $W_{\text{exc}}(f)$ . It is observed as well that such a deviation reflects, on going to the kHz  
 158 range, an important role of the dw processes at low inductions and a decreasing one at high inductions.  
 159 We find, in particular, that about 70 % of the measured loss  $W(f)$  is contributed by  $W_{\text{exc}}(f)$  at 10 kHz  
 160 and  $J_p = 0.25$  T, while for  $J_p = 1.70$  T, 95 % of it is covered at the same frequency by  $W_{\text{class}}(f)$ . To note  
 161 also how the curve  $W_{\text{class}}(f)$  at  $J_p = 0.25$  T versus suffers predictable slope changes with increasing the  
 162 frequency, in qualitative agreement with the corresponding behavior of the permeability at the sheet  
 163 surface  $\mu_{r,\text{surf}}$ .

164 Supporting information regarding the evolution of the magnetization process versus  $f$  and  $J_p$   
 165 can be gained looking directly at the dw dynamics by the stroboscopic Kerr experiments. We provide  
 166 in Figs. 4 and 5 few images taken on a well oriented [001](110) grain at low and high inductions and  
 167 different frequencies. Fig. 4 shows an example of domain structure observed along a semi-cycle taken  
 168 between  $J_p = \pm 0.50$  T at 500 Hz and 10 kHz. A regular oscillatory motion of the walls, including  
 169 bowing, is observed at 500 Hz. But at 10 kHz, near complete disappearance of the dws at the surface  
 170 takes place, following multiplication and strong bowing. The antiparallel  $180^\circ$  dw structure is  
 171 preserved and reappears in full, with denser population with respect the previous case, on the return  
 172 from  $J_p$ . We conclude that at sufficiently low induction the magnetization reversal occurs at high  
 173 frequencies by dw motion and bowing, consistent with the persisting large contribution of  $W_{\text{exc}}(f)$  to  
 174 the measured loss  $W(f)$ . Quite a different picture emerges in Fig. 5 from the Kerr sequence at 5 kHz  
 175 taken along the semi-cycle with  $J_p = \pm 1.70$  T. Starting from the fully saturated surface state observed  
 176 at  $J = J_p$ , oppositely directed domains nucleate and grow at the surface, to eventually form a full reverse  
 177 layer well before attaining the demagnetized state. This process, symmetrically occurring on the  
 178 opposite sheet side, will expectedly proceed by a mechanism close to the front reversal motion  
 179 predicted by the classical model, as sketched in Fig. 2. If this is the case, little loss contribution to the  
 180 measured  $W(f)$  is expected to come from the moving dws, as demonstrated by the faint proportion of  
 181  $W_{\text{exc}}(f)$  predicted in Fig. 3b. This conclusion is further substantiated by the comparisons made between

182 the measured and the classically predicted hysteresis loops, when obtained in the upper  $J_p$ - $f$  right  
 183 corner. We see in Fig. 6 how at 10 kHz and  $J_p = 1.7$  T the loop computed via Eq. (1) and the measured  
 184 one have remarkably close shape and area. The slightly higher area of the experimental loop accounts  
 185 for residual contribution by the dw motion, in agreement with the high-frequency loss behaviour shown  
 186 in Fig. 3b. The slightly re-entrant shape of the experimental loop is related to the threshold field  
 187 required, as shown in Fig. 6, to start the nucleation of the surface domains. It is finally noted the close  
 188 similarity with the hysteresis loop (dashed line) calculated for an ideal step-like constitutive equation.<sup>16</sup>  
 189

#### 190 **IV. Conclusions**

Magnetic losses have been investigated in grain-oriented high-permeability 0.29 mm thick Fe-Si sheet upon a wide range of peak polarization values ( $100 \text{ mT} \leq J_p \leq 1.7 \text{ T}$ ) and frequencies (DC – 10 kHz). The loss properties have been assessed in the framework of the loss separation concept, generalized to cover the skin effect phenomena in the high-frequency region. We aim in this way to retrieve physical information on the broadband magnetization process in materials nowadays exposed to widening applicative areas, while overcoming the limitations of the empirical-phenomenological approaches proposed in the available literature. Looking for a manageable numerical treatment, the actual hysteretic magnetic constitutive equation is approximated with the normal magnetization curve, which is inserted in the Maxwell's diffusion equation. This is solved by a simple finite element algorithm. The macroscopic induction profiles versus sheet thickness as a function of  $J_p$  and  $f$  and the related classical energy loss component are thereby calculated. The familiar phenomenon of propagation of magnetization reversal fronts from the sheet surface to the mid-plane occurring along a semi-cycle is, in particular, retrieved in the upper  $J_p$ - $f$  right corner. With the induction profile and the classical energy loss component  $W_{\text{class}}$  available over the whole frequency range, it is a simple matter to calculate the hysteresis  $W_{\text{hyst}}$  and the excess  $W_{\text{exc}}$  loss components, that is, to evaluate the evolution of the domain wall processes across the  $J_p$ - $f$  matrix. In addition, we substantiate the related information by direct Kerr observations of the domain wall dynamics. We obtain that  $W_{\text{dw}} = W_{\text{exc}} + W_{\text{hyst}}$  prevail at all frequencies over  $W_{\text{class}}$  at the lowest induction values, where the localized eddy currents are the major source of energy dissipation for moderate dw displacements and bowing. The macroscopic eddy current patterns, responsible for  $W_{\text{class}}$ , dominate instead upon increasing  $J_p$  at the highest frequencies, the higher  $J_p$  the broader the frequency range where this occurs. In the limit of high peak polarizations (e.g.  $J_p = 1.7 \text{ T}$ ), the oscillatory motion of the  $180^\circ$  dw transforms, on attaining the kHz range, into a through propagation of magnetization reversals. Consequently,  $W_{\text{dw}}$  becomes negligible and the classical approach is sufficient for a reasonably accurate prediction of the measured losses.



- 193 <sup>1</sup>P. Siano, *Renewable and Sustainable Energy Rev.* **30**, 461 (2014).  
194  
195 <sup>2</sup>H. Ichou, D. Roger, M. Rossi, T. Belgrand, and R. Lemaître, *J. Magn. Magn. Mater.* **504**, 166658 (230120).  
196  
197 <sup>3</sup>M. A. Shamsuddin, F. Rojas, R. Cardenas, J. Pereda, M. Diaz, and R. Kennel, *Energies* **13**, 2319 (2020).  
198  
199 <sup>4</sup>T. Belgrand, R. Lemaître, A. Benabou, J. Blaszowski et C. Wang, *AIP Advances* **8**, 047611 (2018).  
200  
201 <sup>5</sup>G. Parent, R. Penin, J. P. Lecointe, J. F. Brudny, and T. Belgrand, *IEEE Trans. Magn.* **49**, 1977 (2013).  
202  
203 <sup>6</sup>L. Gao, L. Zeng, J. Yang, and R. Pei, *AIP Advances* **10**, 015127 (2020).  
204  
205 <sup>7</sup>K. Foster, F.E. Werner, and R.M. Del Vecchio, *J. Appl. Phys.* **53**, 8308 (1982).  
206  
207 <sup>8</sup>R. Liu and L. Li, *IEEE Trans- Pow. Electr.* **36**, 2009 (2020).  
208  
209 <sup>9</sup>J. Mühlethaler, J. Biela, J. W. Kolar, and A. Ecklebe, *IEEE Trans. Pow. Electr.* **27**, 953 (2012).  
210  
211 <sup>10</sup>C. Appino, G. Bertotti, D. Binesti, O. Bottauscio, M. Chiampi, J.P. Ducreux, F. Fiorillo, M. Repetto, and P.  
212 Tiberto, *J. Appl. Phys.* **79**, 4575 (1996).  
213  
214 <sup>11</sup>L. Dupre, O. Bottauscio, M. Chiampi, M. Repetto, and J. Melkebeek, *IEEE Trans. Magn.* **35**, 4171 (1999).  
215  
216 <sup>12</sup>C. Beatrice, C. Appino, O. de la Barrière, F. Fiorillo, and C. Ragusa, *IEEE Trans. Magn* **50**, 6300504 (2014).  
217  
218 <sup>13</sup>S.E. Zirka, Y.I. Moroz, S. Steentjes, K. Hameyer, K. Chwastek, S. Zurek, and R.G. Harrison, *J. Magn. Magn.*  
219 *Mater.* **394**, 229 (2015).  
220  
221 <sup>14</sup>S. E. Zirka, Y. I. Moroz, P. Marketos, A. J. Moses, D. C. Jiles, and T. Matsuo, *IEEE Trans. Magn.* **44**, 2113  
222 (2008).  
223  
224 <sup>15</sup>C. Serpico, C. Visone, I. D. Mayergoyz, V. Basso, and G. Miano, *J. Appl. Phys.* **87**,. 6923 (2000).  
225  
226 <sup>16</sup>G. Bertotti, *Hysteresis in Magnetism*, Academic Press, San Diego, CA (1998) p. 407.  
227  
228 <sup>17</sup>F. Friedlaender, *Trans. AIEE, Part I* **75**, 268(1956 ).  
229  
230 <sup>18</sup>R. Schaefer, I. Soldatov, and S. Arai, *J. Magn. Magn. Mater.* **474**, 221 (2019).  
231  
232 <sup>19</sup>F. Fiorillo, *Measurement and Characterization of Magnetic Materials*, (Academic-Elsevier, San Diego CA,  
233 2004) p. 362.  
234  
235 <sup>20</sup>O. de la Barriere, C. Ragusa, M. Khan, C. Appino, F. Fiorillo, and F. Mazaleyrat, *IEEE Trans. Magn.* **52**,  
236 2001204 (2016).  
237  
238 <sup>21</sup>G. Bertotti, *IEEE Trans. Magn.* **24**, 621 (1988).  
239  
240 <sup>22</sup>E. Barbisio, F. Fiorillo, and C. Ragusa, *IEEE Trans. Magn.* **40** 1810 (2004).  
241

243  
 244  
 245  
 246  
 247  
 248  
 249  
 250  
 251  
 252  
 253  
 254  
 255  
 256  
 257  
 258  
 259  
 260  
 261  
 262  
 263  
 264  
 265  
 266

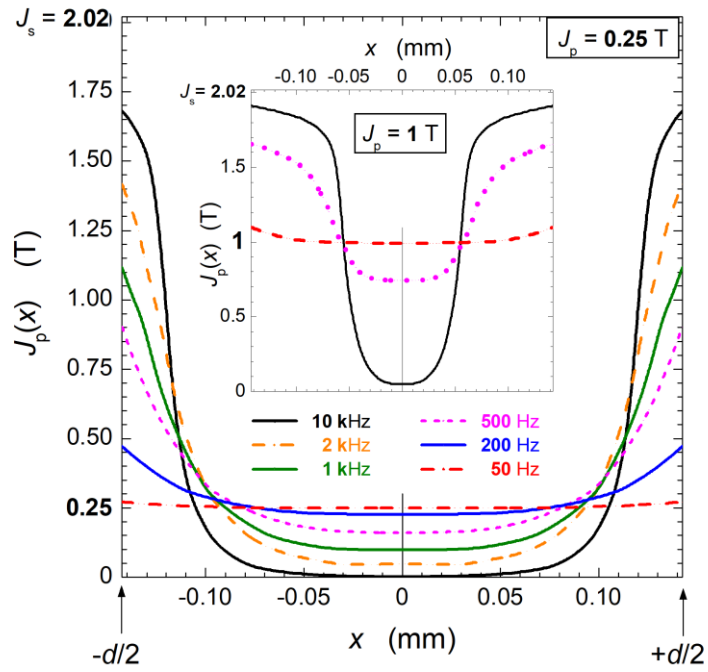


Fig. 1. Calculated profiles of the local peak polarization value  $J_p(x)$  across the 0.29 mm thick GO sheet and their dependence on the magnetizing frequency for average peak polarization  $J_p = 0.25$  T. The inset shows the evolution taken by such profiles for  $J_p = 1.0$  T.

267  
 268  
 269  
 270  
 271  
 272  
 273  
 274

275  
 276  
 277  
 278  
 279  
 280  
 281  
 282  
 283  
 284  
 285  
 286  
 287  
 288  
 289  
 290  
 291  
 292

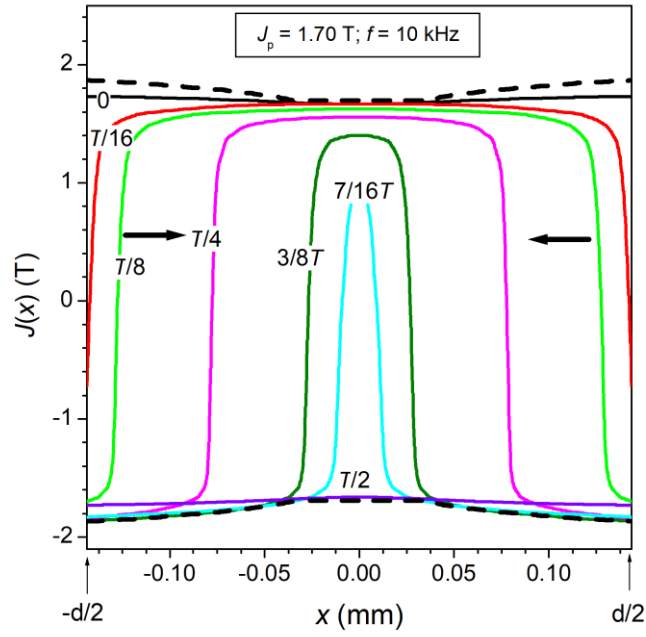


Fig. 2. Reversal fronts symmetrically proceeding inward from the opposite sheet surfaces at high frequencies and high induction values, as predicted to occur by the classical approach in the 0.29 mm GO sheet. The calculations assume a constitutive equation coincident with the normal magnetization curve. The fronts are shown at different instants of time ( $T = 1/f$ ) along a semi-cycle taken at 10 kHz between  $J_p = \pm 1.7$  T. The dashed lines shows the corresponding profile of the peak polarization values  $\pm J_p(x)$ .

293  
 294  
 295  
 296  
 297  
 298  
 299  
 300  
 301  
 302  
 303  
 304  
 305  
 306  
 307  
 308  
 309  
 310  
 311  
 312  
 313  
 314  
 315  
 316  
 317  
 318

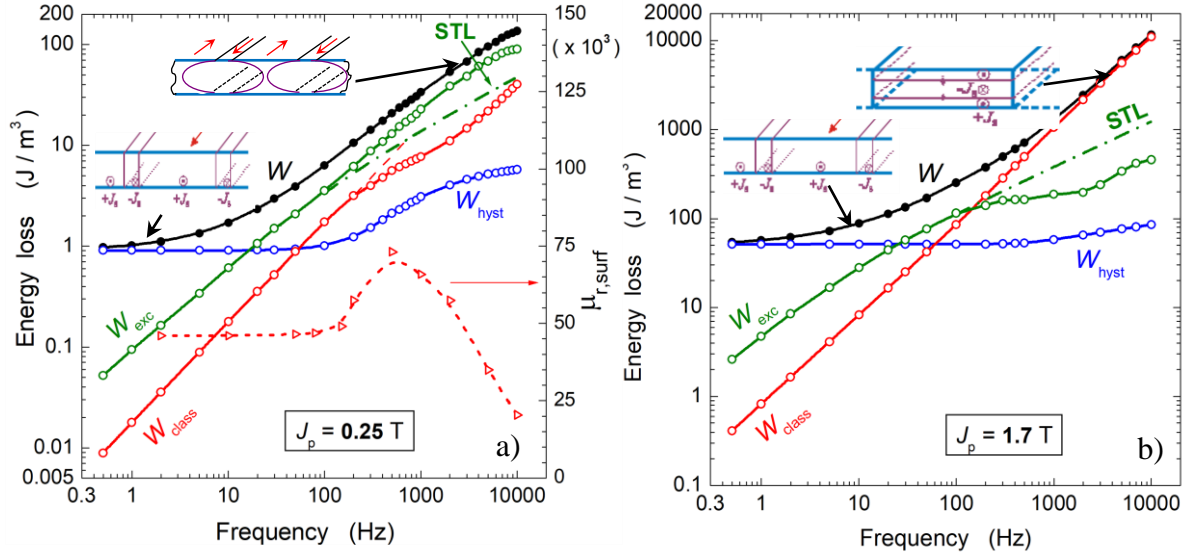


Fig. 3. DC-10 kHz loss decomposition in the 0.29 mm thick GO sheet at low and high inductions. Largely different behaviours of the loss components for  $J_p = 0.25$  T and  $J_p = 1.70$  T take place beyond a few hundred Hz, because of the emerging non-homogeneity of the induction across the sheet thickness. To note the behaviour of the permeability  $\mu_{r,\text{surf}}$  at the sheet surface versus  $f$ , which correlates with the behaviour of  $W_{\text{class}}$ , and the prediction of  $W_{\text{exc}}$  by the statistical theory of losses (STL line), which deviates from the experimental result upon the establishment of the skin effect.

370  
371  
372  
373  
374  
375  
376  
377  
378  
379  
380  
381  
382  
383  
384  
385  
386  
387  
388  
389  
390  
391  
392  
393  
394  
395  
396  
397  
398  
399  
400  
401  
402  
403  
404  
405  
406  
407  
408  
409  
410  
411  
412  
413  
414  
415  
416  
417  
418  
419  
420

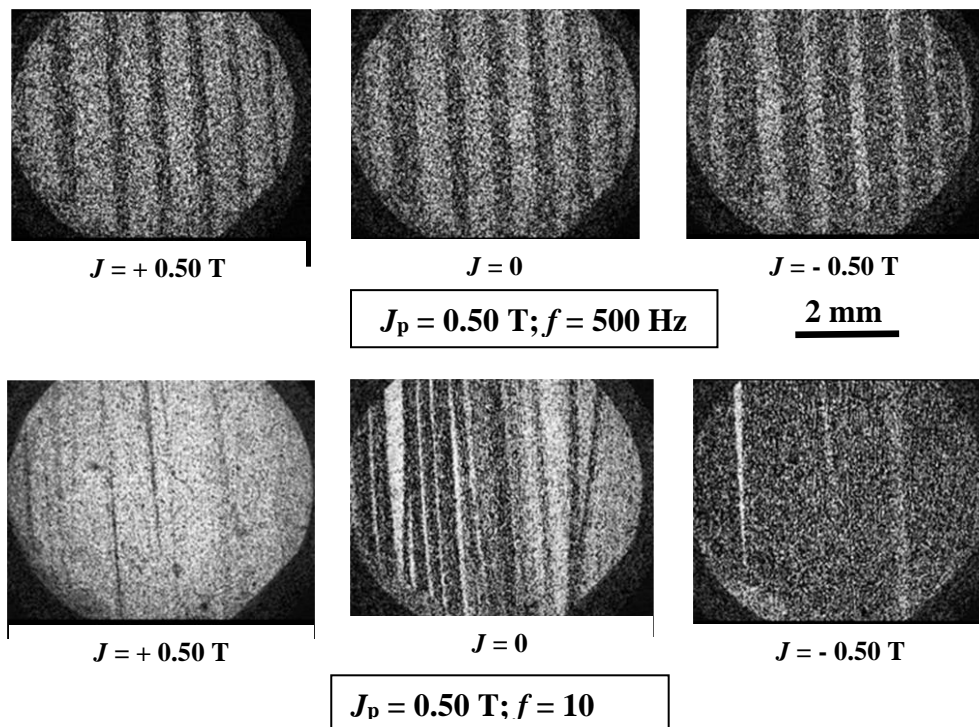


Fig. 4. Domain structure in a well oriented grain and its evolution along a semi-cycle between  $\pm 0,50$  T at 500 Hz and 10 kHz.

421  
422  
423  
424  
425  
426  
427  
428  
429  
430  
431  
432  
433  
434  
435  
436  
437  
438  
439  
440  
441  
442  
443  
444  
445  
446  
447  
448  
449  
450  
451  
452  
453

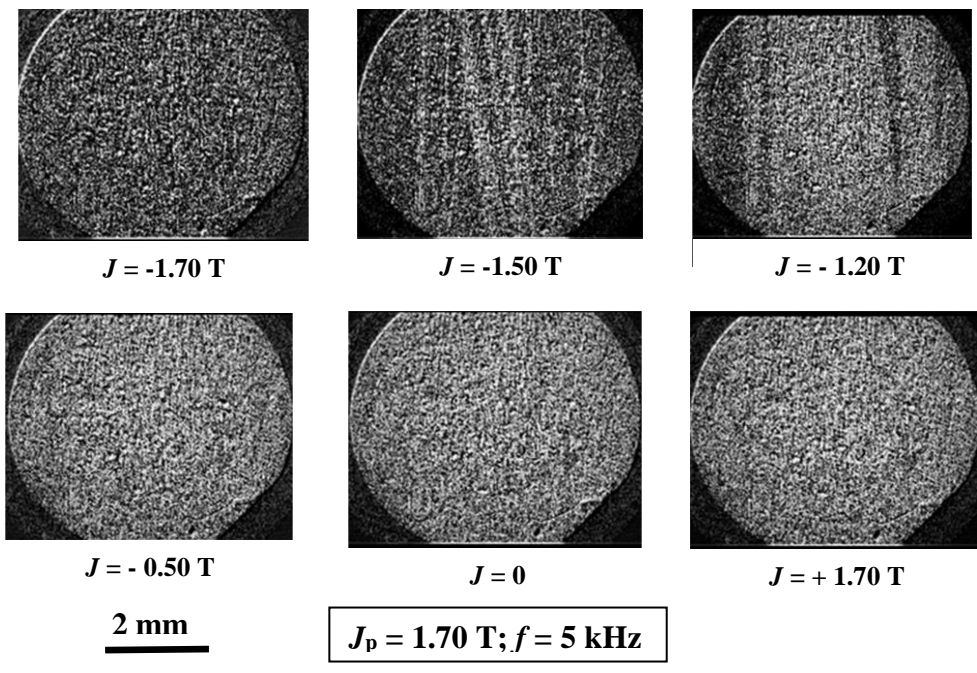


Fig.5. As in Fig. 4 along an ascending semi-cycle run between -1.70 T to +1.70 T at 5 kHz.

454  
455  
456  
457  
458  
459  
460  
461  
462  
463  
464  
465  
466  
467  
468  
469  
470

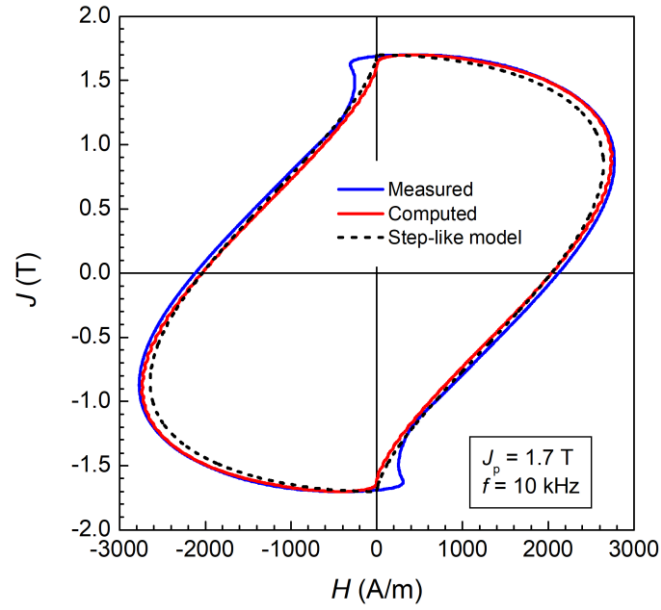


Fig. 6. The hysteresis loop classically computed via the diffusion Eq. (1) compares with the hysteresis loop measured at 10 kHz and  $J_p = 1.70 \text{ T}$ , in good agreement with a magnetization mechanism in the sheet by inward motion of reversal fronts, as sketched in Fig. 2. A faint contribution to dissipation by  $dw$  motion results in a slightly wider experimental loop. To note a threshold mechanism at the beyond the romance point, descending from the nucleation of surface domains, as revealed by the images of Fig. 5. The dashed line is calculated for the ideal case of a step-like constitutive equation ranging between  $\pm 1.85 \text{ T}$ .<sup>16</sup>